JOURNAL OF GEOPHYSICAL RESEARCH, VOL. 102, NO. D14, PAGES 16,935-16,946, JULY 27, 1997

AVHRR remote sensing of aerosol optical properties in the Persian Gulf region, summer 1991

Teruyuki Nakajima and Akiko Higurashi

Center for Climate System Research, University of Tokyo, Tokyo, Japan

Abstract. Satellite remote sensing is studied in this paper for retrieving aerosol parameters, i.e., aerosol optical thickness at 0.5 μm $\tau_{0.5}$, size exponent p, and absorption index κ, from channel 1 and 2 radiances of the NOAA 11 advanced very high resolution radiometer (AVHRR) in the Persian Gulf region in the summer of 1991. Results of the remote sensing are compared with ground-based values obtained from solar radiation measurements with a sunphotometer and a pyranometer in Bushehr, Iran. It is found that tuning the calibration coefficients of AVHRR and introduction of a suitable aerosol absorption are needed for a good agreement between satellite-derived and ground-based values of $\tau_{0.5}$. The aerosol absorption index is also retrieved with two methods, i.e., simultaneous analyses with ground-based $\tau_{0.5}$ and p, and the Fraser-Kaufman method. Retrieved values of the aerosol single-scattering albedo are $\omega \approx 0.75$ and 0.70 from the two methods, respectively, for the Kuwait oil-fire smoke layer. The single scattering albedo of another case, which is regarded as a sand-dust layer, is estimated to be $\omega \approx 0.76$ with the Fraser-Kaufman method.

1. Introduction

There has been recent recognition that anthropogenic aerosols have a substantial effect on our climate [*Mitchell et al.*, 1995]. *Charlson et al.* [1992] evaluated the radiative forcing of anthropogenic aerosols through direct and indirect effects as large as -2 W m^{-2} for the aerosol increase after the industrial revolution. Recent evaluations of the direct effect, however, have a wide range from -0.3 W m^{-2} to -0.9 W m^{-2} [*Kiehl and Briegleb*, 1993; *Taylor and Penner*, 1994; *Kiehl and Rodhe*, 1995], indicating the estimation of aerosol effects is difficult. There will be a 20% to 30% reduction of radiative forcing if we count black carbon particles in the evaluation [*Penner*, 1995].

The indirect effect of aerosols is a further uncertainty, even though the finding of the ship trail cloud phenomenon [*Coakley et al.*, 1987; *Radke et al.*, 1989] has prompted new discussion on the large-scale change of the microphysical state of maritime low-level clouds by injection of anthropogenic cloud condensation nuclei (CCN). There has been a significant effort, in this situation, for developing algorithms to obtain cloud optical thickness and effective particle radius of water clouds from satellites [*Nakajima et al.*, 1991; *Han et al.*, 1994; *Nakajima and Nakajima*, 1995. *Han et al.* [1994] has shown that the northern hemispheric cloud particle radius is smaller than that of the southern hemisphere, suggesting the global statistics of cloud microphysics are more or less controlled by CCN concentration. On the other hand, *Kaufman and Nakajima* [1993] have found that it is possible for continental clouds to reduce their reflectivity through interaction with light-absorbing aerosols. This is caused by an enhanced light absorption due to multiple scattering inside the cloud layer. Their estimation of the absorption index (the imaginary part of the complex refractive index) of smoke aerosols is in the range of 0.02-0.03. This value is similar to that of anthropogenic aerosols in turbid atmospheres of Asian urban areas [*Tanaka et al.*, 1983; *Qiu et al.*, 1987; *Tanaka et al.*, 1990; *Hayasaka et al.*, 1992]. Similar reduction of cloud reflectivity is therefore possible in such areas.

The above discussion indicates that satellite remote sensing of aerosol optical characteristics is important for studying the direct and indirect effects of aerosols on the global climate. There are useful retrievals of aerosol optical thickness from the advanced very high resolution radiometer (AVHRR) generated by NOAA [*Stowe et al.*, 1992]. This NOAA algorithm has considerable room, however, for further improvement. First of all, it is important to extend their one channel algorithm to a multichannel algorithm for getting parameters for aerosol size distribution as well as the optical thickness. In this issue we can learn the skills of atmospheric correction algorithms of the ocean color community for application to ocean color sensors [*Gordon and Morel*, 1983; *Gordon and Wang*, 1994], such as the Nimbus 7 coastal zone color scanner (CZCS), Sea-viewing Wide-Field-of-view Sensor (SeaWiFS), and the Advanced Earth Observing Satellite (ADEOS) Ocean Color and Temperature Sensor (OCTS), which have several sensitive channels in the visible spectral region. It is possible to get aerosol parameters similar to Ångström parameters from these channels as these authors have proven. The absorption index is another important parameter in remote sensing and climate issues, which may be retrieved from satellite remote sensing as proposed by *Fraser and Kaufman* [1985].

Paper number 96JD01935.
0148-0227/97/96JD-01935$09.00

In this paper, we discuss remote sensing of aerosol optical parameters using AVHRR channels 1 and 2 in the Persian Gulf region in the summer of 1991. In this period, *Nakajima et al.* [1996a] performed a solar radiation experiment in Iran for studying the Kuwait oil-fire smoke effect and the regional air quality in Iran. In this experiment, daily measurements of direct and diffuse solar radiation were made for the period of June 12 to September 17, 1991, in Bushehr, Iran, to retrieve aerosol optical parameters. The Persian Gulf region at this time had complex aerosol sources, including a large loading of smoke aerosols from Kuwait oil-well fires, heavy sand-dust loading [*Duce*, 1995] and anthropogenic sulfate emission [*Langner et al.*, 1992]. *Rao et al.* [1988] reported a large concentration of soil-derived aerosols in this region observed by AVHRR satellite images. In this study we will compare satellite-derived and ground-based aerosol parameters, i.e., aerosol optical thickness, an index of size distribution, and absorption index, for validating the satellite retrievals.

2. Aerosol Effects on Satellite-Received Radiances

NOAA 11 AVHRR radiances are used in this study for retrieving aerosol parameters. In order to compare satellite-received radiances with theoretical values, we simulate satellite-received radiances by solving a radiative transfer problem in a coupled atmosphere-ocean system. For this purpose we use a general transfer package R-star in the System for Transfer of Atmospheric Radiation (STAR) series, which have been developed by the University of Tokyo and Munich University. The R-star package is an assembly of the algorithms of *Nakajima and Tanaka* [1983, 1986, 1988] with a Lowtran 7 gas absorption model [*Kneizys et al.*, 1986]. There is other package, UV-star, for shortwave calculations with a user-friendly interface [*Ruggaber et al.*, 1994].

Response functions of NOAA 11 AVHRR channels are considered by integrating simulated monochromatic radiances at 10 wavelengths in the spectral bands of channel 1 (with band center wavelength at $\lambda = 0.63$ μm) and channel 2 ($\lambda = 0.84$ μm) [*Kidwell*, 1988]. To take into account the water vapor and ozone absorption, the Air Force Geophysics Laboratory (AFGL) middle-latitude summer atmosphere model is assumed in our calculations. It has been confirmed by numerical experiments that an error involved in the assumed model atmosphere is small because of the large aerosol signal we are investigating. A ruffled ocean surface reflection with surface wind velocity of 5 m s^{-1} or Lambert reflection surface is assumed, depending on surface conditions, but the upwelling radiance from the ocean body is neglected, since this effect is not large in those channels with strong light absorption by water molecules and with relatively heavy aerosol loading.

Figures 1 and 2 show the theoretical relationship between apparent reflectances in two channels, R_1 and R_2, at the mean Earth-Sun distance, defined as

$$R_i(\theta,\theta_0,\phi) = \frac{\pi L_i(\theta,\theta_0,\phi)\rho^2}{F_i \cos\theta_0}. \quad (1)$$

where L_i and F_i are band-integrated satellite radiance and solar insolation respectively, at the top of the atmosphere in the ith channel of AVHRR; θ_0 is the solar zenith angle; θ is the nadir angle of emergent rays; ϕ is the azimuthal angle of the emergent ray relative to the solar direction; ρ is the Earth-Sun distance in astronomical units. Simulated conditions are of July 17 and September 1 on a sea area off the coast of Bushehr, Iran (50.8°E, 29.0°N, 10 *m* mean sea level (MSL)), where *Nakajima et al.* [1996a] performed ground-based solar radiation measurements. Table 1 summarizes reflectances and angular parameters of our AVHRR imagery analyses. Aerosol parameters obtained by *Nakajima et al.* [1996a] are also listed in Table 1.

We select three parameters for modeling aerosol optical characteristics, i.e., κ, $\tau_{0.5}$, and p, as shown in Figures 1 and 2. The first parameter is the absorption index defined as the magnitude of the imaginary part of the aerosol complex refractive index $m = n - \kappa i$. The parameter $\tau_{0.5}$ is the aerosol optical thickness at $\lambda = 0.5$ μm and p is the power of the power-law number size distribution of aerosols as a function of particle radius r,

$$\frac{dn}{dr} = \begin{cases} Cr^{-p} & 0.1 < r \le 10\mu\text{m} \\ const & r \le 0.1\mu\text{m} \end{cases}. \quad (2)$$

With this aerosol model, we can calculate parameters for radiation transfer by the Mie theory, i.e., the spectral optical thickness τ_λ, single-scattering albedo ω_λ, and scattering phase function of aerosols. The following relationships are found with the maximum particle radius of 10 μm for radius integration in Mie theory calculations:

$$\tau_\lambda = \tau_{0.5}(\lambda/0.5)^{-\alpha}, \quad (3)$$

and

$$p = 2.76 + 1.35\alpha. \quad (4)$$

We hereafter refer to $\tau_{0.5}$ and p as turbidity parameters or the aerosol optical thickness (without specifying the reference wavelength at 0.5 μm) and the size exponent, respectively. The aerosol layer is assumed to be homogeneous and located between 1 km and 3 km in height.

It is found from Figures 1 and 2 that the relationship is much different between the two figures. The angular condition of September 1 (Figure 2) shows that the studied area is inside the sun glitter ($\theta \approx \theta_0$, $\phi \approx 0$), and in this case, R_1 and R_2 are not a monotonic function of the turbidity parameters unless $\tau_{0.5} \ge 2$ and $p \ge 4$, in which case the atmospheric path radiance becomes dominant as compared with the surface-reflected radiance. This indicates that it is difficult to estimate the aerosol optical thickness and the size exponent in sun glitter conditions. Outside the sun glitter, as on July 17 (Figure 1), on the other hand, R_1 and R_2 are a monotonic function of the turbidity parameters, so that $\tau_{0.5}$ and p can be retrieved from channel 1 and 2 reflectances without difficulty.

The reflectance also depends on the aerosol complex refractive index $m = n - \kappa i$. In particular, the absorption index κ has a large range and is difficult to set properly for successful retrievals of turbidity parameters. Figure 3 simulates apparent reflectances of nine selected cases with p = 3, 4, 5; $\tau_{0.5}$= 0.4, 1.0, 2.0; and κ= 0.01, 0.02, and 0.03 for the angular condition of July 17. The real part of the refractive

Table 1a. Imagery Information for NOAA11 AVHRR Local Area Coverage (LAC) Data Sets

Date in 1991	Time	Corner Locations, deg				θ_0, deg	θ, deg	ϕ, deg	R_1, %	R_2, %	Comment
June 12	1107	(38N,	25E)	(19N,	62E)	34.9	37.0	173.8	4.63	2.37	
June 15	1032	(38N,	33E)	(19N,	71E)	27.2	21.6	5.3			Sunglitter
June 22	1053	(38N,	28E)	(19N,	66E)	31.2	13.4	173.6	7.60	6.45	
June 24	1030	(34N,	36E)	(19N,	72E)	26.1	26.8	5.4			Sunglitter
July 2	1039	(34N,	34E)	(19N,	70E)	27.8	13.7	5.0			Sunglitter
July 8	1111	(34N,	26E)	(19N,	62E)	34.7	38.3	174.9	8.69	6.37	
July 17	1108	(34N,	27E)	(19N,	63E)	34.3	33.4	177.3	8.00	5.09	
July 25	1117	(34N,	25E)	(19N,	61E)	36.6	43.4	179.4	11.48	8.22	
Aug. 4	1102	(34N,	29E)	(19N,	65E)	34.6	22.0	176.1	7.60	5.11	
Aug. 12	1111	(34N,	27E)	(19N,	63E)	37.8	33.8	173.3	8.70	6.06	
Aug. 15	1035	(38N,	34E)	(19N,	71E)	31.2	24.8	11.7			Sunglitter
Aug. 20	1119	(38N,	23E)	(19N,	61E)	41.2	43.7	170.9	9.07	6.57	
Sept. 1	1041	(34N,	35E)	(19N,	71E)	36.0	19.4	17.6			Sunglitter
Sept. 10	1037	(38N,	34E)	(19N,	72E)	38.2	26.1	21.6			Sunglitter
Sept. 15	1121	(34N,	25E)	(19N,	61E)	47.9	42.9	161.9	9.53	6.54	

Date, starting time, and locations of upper right and lower left corners of images in Plate 1 are shown together with solar zenith angle θ_0, satellite zenith angle θ, and azimuthal angle of the satellite relative to the Sun ϕ; R_1 and R_2 are apparent reflectances of channels 1 and 2 in percent with $S_1 = 0.114$ and $S_2 = 0.122$ in (5). Indicated times are Iranian standard time (subtract 4.5 hours to get universal time).

index is fixed at a typical value of 1.5. The figure shows that the dependence of R_1 and R_2 on κ is similar to that on $\tau_{0.5}$ and hence the separation of the information of optical thickness and absorption is difficult. We have to know one of the parameters, $\tau_{0.5}$ or κ, to retrieve the other parameter.

3. Simultaneous Analyses With Ground-Based Aerosol Parameters

To help in the analyses of AVHRR reflectances, we use ground-based turbidity parameters and the absorption index derived from solar radiation measurements in the summer of 1991 (June 12 to September 17, 1991) in Bushehr [*Nakajima et al.*, 1996a]. Turbidity parameters $\tau_{0.5}$ and p were derived from direct spectral solar irradiance measurements by a sunphotometer and also the absorption index κ from diffuse and total solar radiative fluxes measured by a pyranometer. Figure 4 shows the time series of turbidity parameters and absorption index derived in this way. Increases in the aerosol optical thickness occurred almost every week in June. The associated absorption index was estimated to be larger than 0.05 and the single-scattering albedo of aerosols was less than 0.7. *Nakajima et al.* [1996a] concluded, taking into account the aerosol optical characteristics thus obtained, as well as air mass trajectories and AVHRR images, that these increases in $\tau_{0.5}$ and κ were caused by intrusion of oil-fire smoke mostly due to the breakdown of strong seasonal northwest wind in this season.

The flow pattern of oil-well fire smoke has been intensively investigated by trajectory analyses and satellite imagery [*Cahalan*, 1992; *Limaye et al.*, 1992; *McQueen and Draxler*, 1994; *Husain*, 1994]. The dominant flow pattern was along a narrow region of the Persian Gulf coast line of Saudi Arabia, as shown in the case of June 12 in Plate 1. *Nakajima et al.* [1996a] pointed out that the aerosol optical thickness at Bushehr was small when this steady northwesterly seasonal wind system dominated, whereas the aerosol optical thickness became large almost once a week when the seasonal wind broke down and the smoke layer spread around the smoke source relatively isotropically, as in the case of June 22 in Plate 1. Wind speed was generally weak in the latter case. According to *Husain* [1994], a simulation of SO_2

Table 1b. Ground-Based Values of τ, p, ω, and κ Obtained by *Nakajima et al.*[1996a]

Date in 1991	Time	τ	p	ω	κ
June 12	1630	0.1610	4.0120	0.8491	0.0515
June 15	1625	1.3570	3.6470	0.6630	0.0684
June 22	1530	1.8530	3.6660	0.6786	0.0620
June 24	1530	0.5310	4.1130	0.8296	0.0258
July 2	1530	0.8790	4.0430	0.7096	0.0584
July 8	1530	0.8730	3.6170	0.8307	0.0178
July 17	1530	0.5290	3.4640	0.9246	0.0043
July 25	1530	0.8340	3.4550	0.8312	0.0146
Aug.4	1530	0.7690	3.8940	0.8141	0.0262
Aug.12	1530	0.9230	3.4420	0.7829	0.0224
Aug.15	1530	0.6820	3.8970	0.8346	0.0216
Aug.20	1530	1.2750	3.8070	0.6988	0.0576
Sept.1	1530	0.6850	3.9240	0.7925	0.0318
Sept.10	1530	0.3240	4.3080	0.8654	0.0201
Sept.15	1530	0.8770	4.0200	0.7689	0.0393

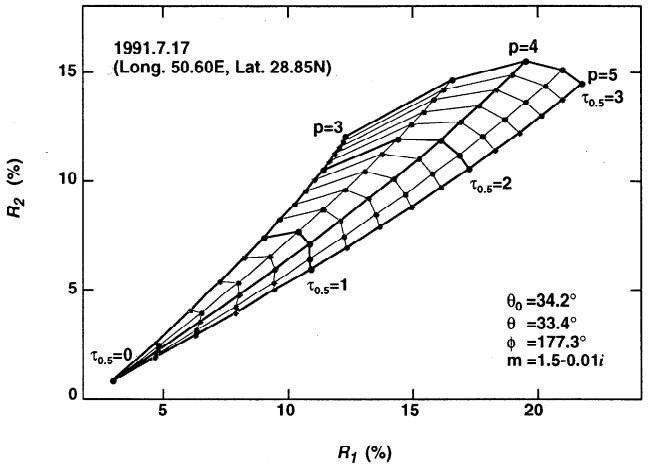

Figure 1. Relationship between AVHRR channel 1 and 2 apparent reflectances (%) for various optical thicknesses $\tau_{0.5}$ and size exponents p. The angular geometry of July 17, 1991, is assumed.

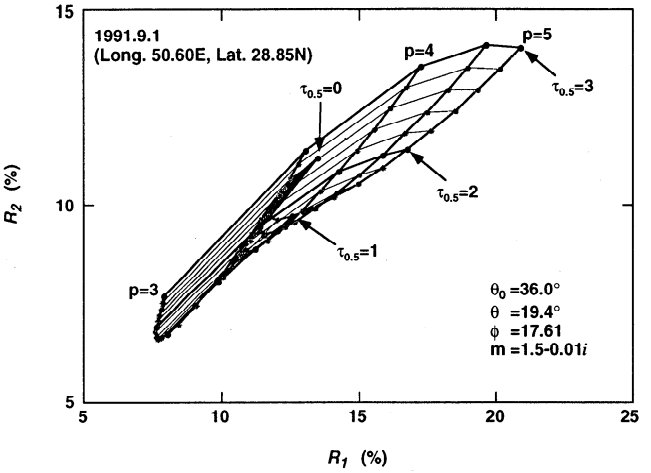

Figure 2. Samc as Figure 1 but for September 1, 1991. The region is in a sun glitter.

concentration and soot deposition, which arc integrated from March to October, indicates the value at Bushehr should be 5 to 10 times smaller than that around Qatar. This value seems to be consistent with the frequency of increases in optical thickness.

Superimposed symbols in Figure 4 show turbidity parameters retrieved from the satellite, assuming three aerosol absorption indices $\kappa = 0.01$, 0.02, and 0.03 for nine AVHRR images. To derive the reflectance in (1), we assume the following formula recommended by NOAA:

$$R_i = \frac{S_i (C_i - C_{i0})}{\cos\theta_0} \ (\%) \cdot \qquad (5)$$

where C_i is the digital count of the ith channel of NOAA 11 AVHRR. Calibration coefficients S_i depend on days after satellite launch owing to deterioration of the radiometer. Adopting the formula of *Kaufman and Holben* [1993], we assume $S_1 = 0.114$ and $S_2 = 0.122$ for the summer of 1991. We refer to these calibration coefficients as the original calibration coefficients. The deep space counts C_{10} and C_{20} are fixed as 40 counts. Table 1 lists reflectance values of the nine cases thus obtained. Plotting these satellite-observed reflectances in figures similar to Figure 1, we can estimate satellite-derived values of $\tau_{0.5}$ and p. We could not find reliable values in the sun glitter cases of Table 1 and have omitted those from the analyses. Figure 4 indicates that there are similarities between ground-based and satellite-derived values of turbidity parameters. It is found, however, that there is a large uncertainty in estimating satellite values unless the aerosol absorption index is assigned in the proper way.

In Figures 5-7 we compare the ground-based turbidity parameters with satellite-derived values with several different assumptions in the retrievals. Figure 5 shows satellite-derived $\tau_{0.5}$ and p retrieved with an assumption $\kappa = 0$, which has been adopted in the NOAA algorithm. It is found that the ground-based $\tau_{0.5}$ and p are largely underestimated by satellite retrievals. *Ignatov et al.* [1995] found a similar situation in that $\tau_{0.5}$ values from their shipborne sunphotometry in 1989 and 1991 were about 2 times larger than their NOAA 11 AVHRR retrievals. They assumed $C_{10} = 40$ and $S_1 = 0.110$ in their analyses, which are very similar to the assumption adopted in Figure 5. To overcome their problem, they needed to increase the absorption index from 0 to 0.01. Figure 6 shows a comparison similar to that in Figure 5 but using the ground-based absorption index for satellite analyses. In this case, ground-based turbidity parameters are slightly overestimated by the satellite, contrary to the result of Figure 5. Comparison of Figsures 5 and 6 suggests that it is possible to find the best fit with an absorption index between zero and ground-based values. Although not shown in the figures, we found the best fit is realized if we decrease the ground-based κ by a factor of 2.

Another way to overcome our problem is to tune the calibration coefficients so as to get good agreement between satellite-derived and ground-based turbidity parameters. One possible solution is given in Figure 7 with $S_1 = 0.093$ and $S_2 = 0.094$. We refer to these calibration coefficients as tuned

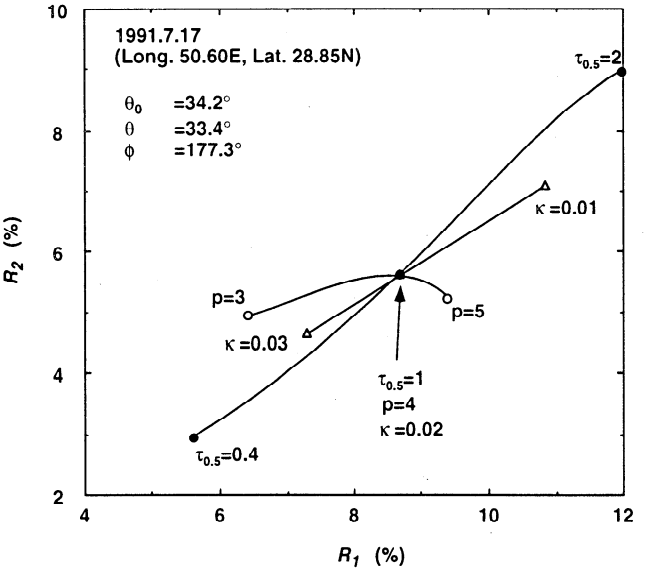

Figure 3. Dependence of AVHRR channel 1 and 2 reflectances on $\tau_{0.5}$ (solid dots), p (open circle), and κ (open triangles).

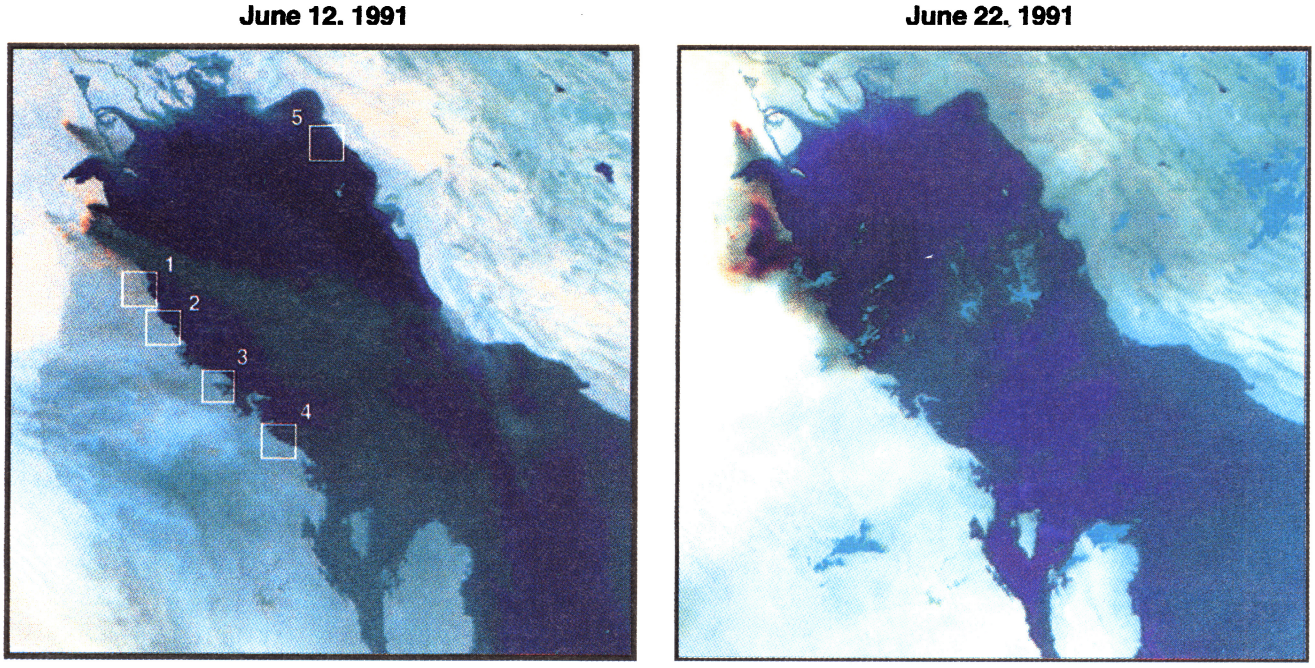

Plate 1. Two distinct flow patterns of oil-fire smoke obtained by NOAA 11 AVHRR imagery over the Persian Gulf region on June 12 and June 22, 1991. Numbered boxes show the areas for Fraser-Kaufman method analyses.

calibration coefficients. The figure shows that there is good agreement between satellite-derived and ground-based values of $\tau_{0.5}$ with one exception at $\tau_{0.5,\,\mathrm{ground}} \approx 2$, which corresponds to an intensive oil-fire smoke layer. One possible reason for this exception is an underestimation of the aerosol optical thickness of the very thick smoke layer by ground-based sunphotometry. The local observer of the sunphotometer reported that it was not able to measure direct solar irradiance by the sunphotometer in cases of very heavy oil-fire smoke layers. This suggests our ground-based measurements tend to underestimate the mean aerosol optical thickness of oil-fire smoke layers over Bushehr.

As for the difference in the size exponent p in Figure 7, it is possible to get a better size exponent by tuning calibration coefficients so as to increase the ratio S_2/S_1, as understood from Figure 1. In this case, however, the satellite-derived optical thickness $\tau_{0.5,\mathrm{sat}}$ starts deviating from the ground-based one $\tau_{0.5,\mathrm{ground}}$. This suggests there may be some inconsistency in $\tau_{0.5,\,\mathrm{ground}}$ and p_{ground} to interpret our satellite radiance model.

Alternatively from the above mentioned method, it is possible to obtain the satellite-derived absorption index assuming $\tau_{0.5,\mathrm{ground}}$ and p_{ground} for simulating satellite radiances. Figure 8 illustrates the idea of this retrieval. In the figure, satellite-derived values $(\tau_{0.5}, p)_{\mathrm{sat}}$ are plotted assuming several values of κ. The open circle shows the ground-based data $(\tau_{0.5}, p)_{\mathrm{ground}}$. Three different candidates are found for the optimal satellite-derived κ in this plot. If we believe $\tau_{0.5,\mathrm{ground}}$, we get point A along the constant $\tau_{0.5}$ line; likewise, point B along the constant p line is obtained if we believe p_{ground}. Figures 1, 3, and 8 show that $\tau_{0.5}$ has more information on κ than p, so that point A might be more reliable. However, an accurate estimation of $\tau_{0.5}$ is more difficult than p in ordinary sunphotometry. It is possible therefore to determine the optimal value at point C, which can be found in order to minimize the relative error in both $\tau_{0.5}$ and p. We thus define three methods, τ, p, and $2D$ for the points A, B, and C, respectively. Figures 9 and 10 compare ground-based values with three possible values of κ and the single-scattering albedo ω thus obtained from the satellite. We have assumed in the calculations the tuned calibration coefficients $S_1 = 0.093$ and $S_2 = 0.094$. An overall agreement with ground-based values is found regardless of methods with two exceptions of large absorption. Significant disagreement in the large values may be due to an underestimation of ground-based optical thickness of the oil-fire smoke layer as explained above. An inconsistency of $\tau_{0.5,\,\mathrm{ground}}$ and p_{ground} found in Figure 7 is not fatal for the satellite retrievals of κ in Figures 9 and 10 with the tuned calibration coefficients. Although not shown in the figures, the three methods estimate very different values from ground-based values if $S_1 = 0.114$ and $S_2 = 0.122$ are assumed.

4. Application of Fraser-Kaufman Method

The study in the preceding section has shown that it is very useful to have ground-based turbidity parameters for retrieving the aerosol absorption index from satellites. This method cannot be applied, however, over areas without ground support data. *Fraser and Kaufman* [1985] has proposed an interesting method for retrieving the absorption index using a contrast of ground surface reflectance. The idea is that a black light-absorbing aerosol layer changes the apparent reflectance over a high-reflecting surface, whereas it does not significantly change the reflectance over a low-reflecting a surface. On the other hand, a white transparent aerosol layer changes the reflectance over a low-reflecting surface, whereas it does not change the reflectance over a high-reflecting surface. The Fraser-Kaufman method finds

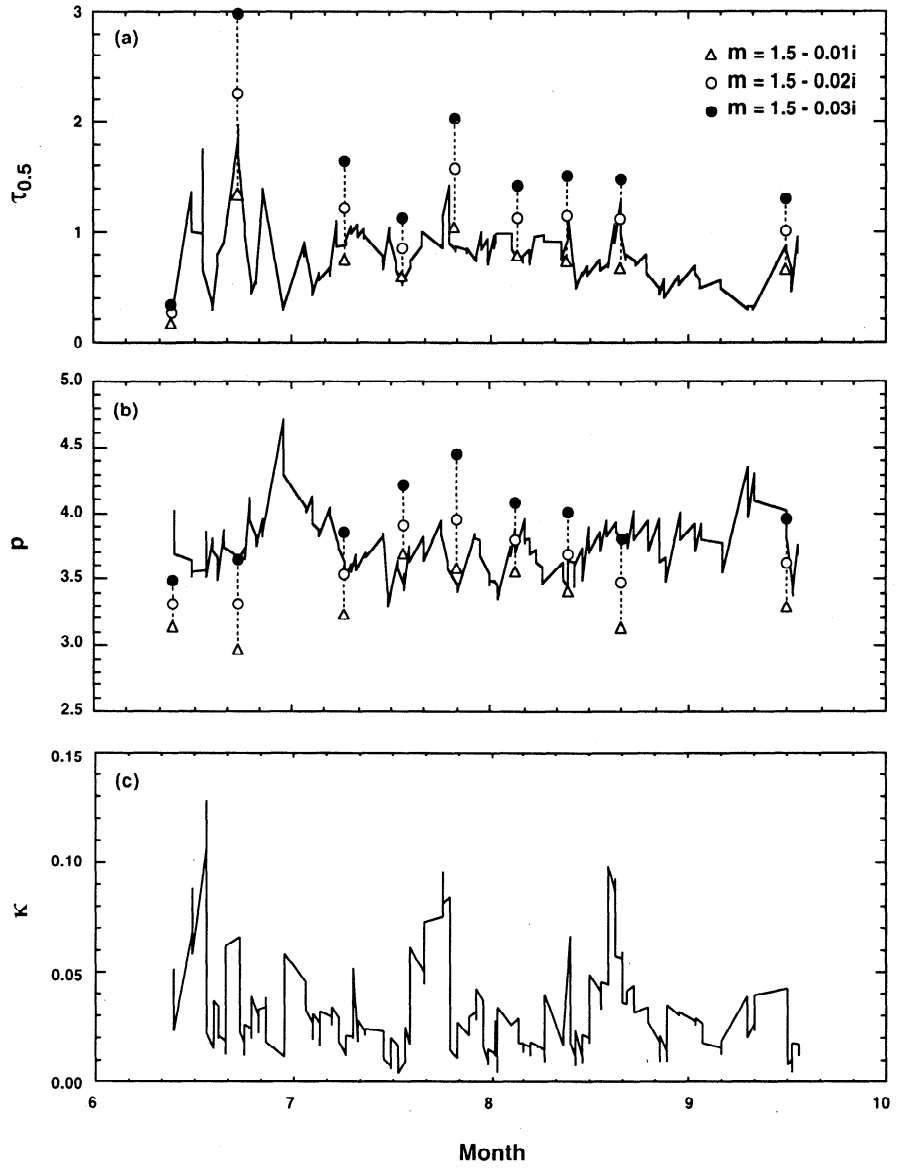

Figure 4. Time series of turbidity parameters (a)$\tau_{0.5}$, (b)p, and (c)κ derived from ground-based solar radiation measurements (reproduced from *Nakajima et al.* [1996a]). Symbols show satellite-derived turbidity parameters from AVHRR with different assumption of κ.

a neutral surface reflectance with which there is no change in the apparent reflectance of the aerosol-laden atmosphere. By adding theory of two layers [*Plass et al.*, 1973], we have the following expression for the deviation of apparent reflectance from the surface albedo A_g:

$$\Delta R \equiv R - A_g = R_A - A_g + T_A(1 - A_g R_A)^{-1} A_g T_A$$

$$\approx R_A - (1 - T_A^2)A_g, \tag{6}$$

where R_A and T_A are reflection and transmission functions, respectively, and an angular integration is implied with a product of two functions in (6). To derive the last equation in (6), reflection and transmission functions are roughly. approcximated by scalars and have neglected terms of $O(A_g^2)$. Equation (6) gives the neutral reflectance as

$$R_0 \approx \frac{R_A}{1 - T_A^2} \tag{7}$$

Since R_A almost linearly depends on $\tau_{0.5}$ [*Gordon and Wang*, 1994], we may have the following approximation,

$$R_A \approx c\,\tau_{0.5} \qquad 1\text{-}T_A^2 \approx 2k\tau_{0.5}, \tag{8}$$

where the slope c and a diffusion coefficient k depend on the aerosol absorption index. Equations (7) and (8) suggest that the neutral reflectance will depend on the aerosol absorption index without significant dependence on the aerosol optical thickness.

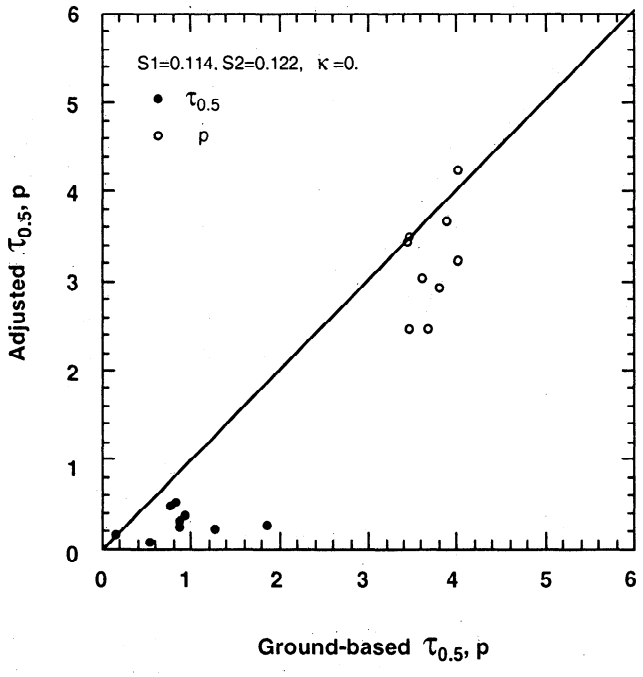

Figure 5. Comparison of satellite-derived turbidity parameters with ground-based values. The absorption index κ=0 is assumed.

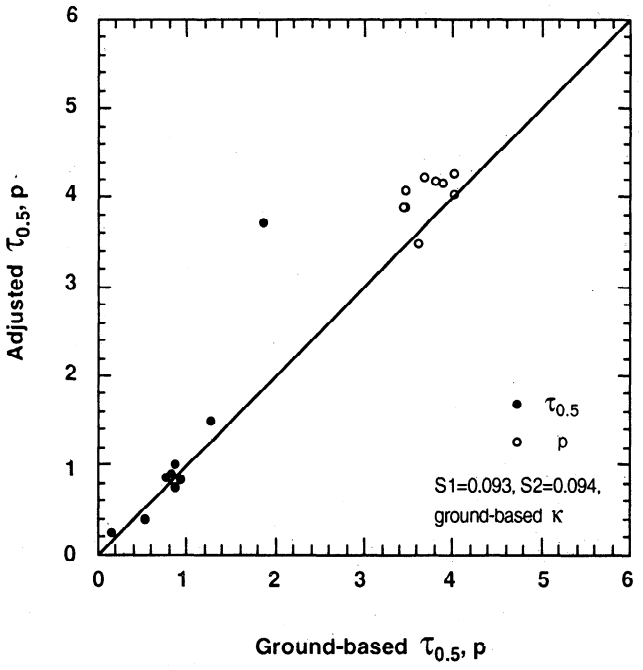

Figure 7. Same plot as in in Figure 6 but with tuned calibration coefficients $S_1 = 0.093$ and $S_2 = 0.094$.

The above mentioned idea can be realized in satellite data analyses by a scatter plot of apparent reflectances of clear and hazy days as shown in Figure11. We have simulated apparent reflectances with different ground albedos (A_g = 0, 0.1, 0.2, 0.3, and 0.4) with three absorption indices κ = 0, 0.01, and 0.05. Parameter $\tau_{0.5,\,clear}$ = 0.05 is assumed for calculating clear-sky reflectances R_{clear}, and two optical thicknesses, $\tau_{0.5,\,hazy}$ = 0.5 and 1.0, are assumed for calculating hazy day reflectances R_{hazy} to make two lines for each absorption index in Figure11. Since the clear-sky reflectance is mostly dependent on the ground albedo, as shown in Figure11, the horizontal axis can serve as an index of surface reflectance in the Fraser-Kaufman method. The figure shows that the neutral reflectance R_0 (= R_{hazy} = R_{clear}) depends on the

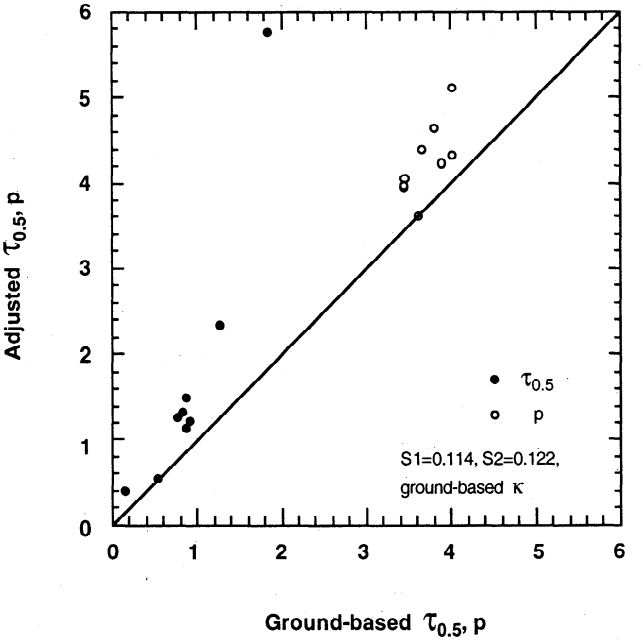

Figure 6. Same plot as in Figure 5 but for satellite retrievals with ground-based absorption index.

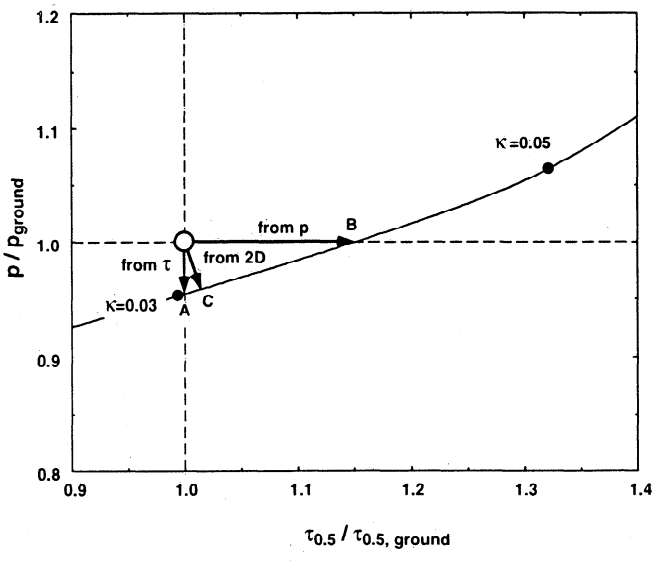

Figure 8. Determination of the aerosol absorption index from a plot of satellite-derived $\tau_{0.5}$ versus p assuming various absorption indices. Open circle shows the observed point. There are three possible candidates for the absorption index, depending on how ground-based parameters are used for the retrieval.

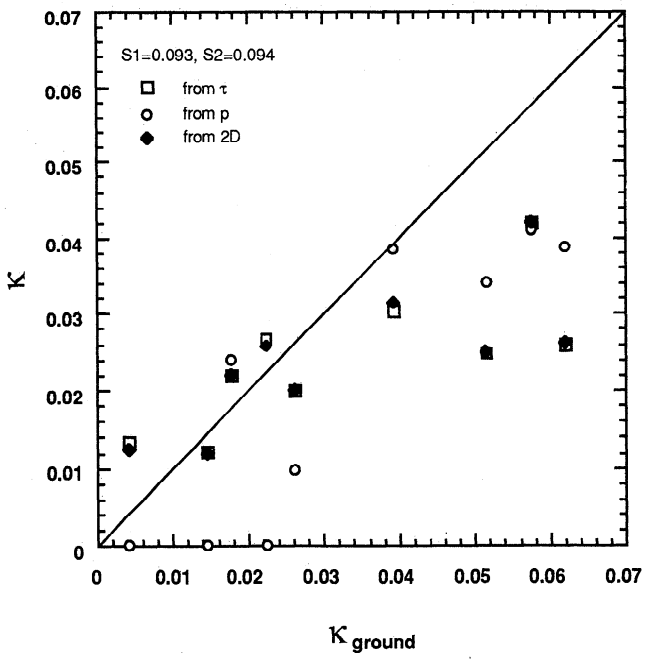

Figure 9. Comparison of satellite-derived absorption index with ground-based values from three different with S_1=0.093 and S_2=0.094. Values are shown from three methods, *τ, p, and 2D*, which are defined in Figure 8.

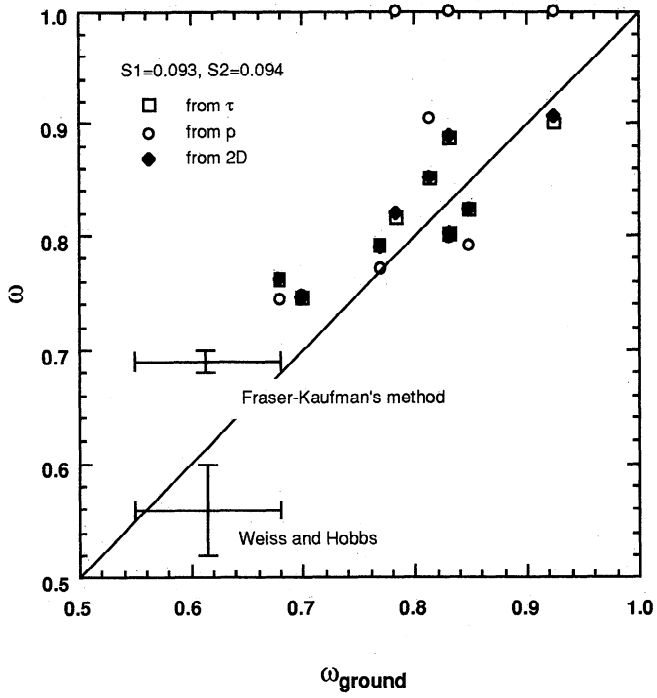

Figure 10. Same as Figure 9 but for aerosol single-scattering albedo. Values obtained by Fraser-Kaufman method and by *Weiss and Hobbs* [1992] are also plotted.

aerosol absorption and does not depend significantly on the optical thickness, as expected from (7) and (8). More precisely, the neutral reflectance depends almost uniquely on aerosol single-scattering albedo, since an inherent variable for radiative transfer is the single-scattering albedo rather than the absorption index. Figure 12 shows how the neutral reflectance depends on the aerosol single-scattering albedo, but does not depend significantly on the assumed aerosol size distribution.

We plot in Figure 11 real AVHRR data of oil-fire smoke over the high-reflecting desert area of Saudi Arabia and the low-reflecting Persian Gulf sea surface designated as location 4 in Plate 1. To cover various underlying surface albedos, we have sampled pixels from the entire region of the square across the desert and sea. The figure shows that it is possible to find the neutral reflectance from AVHRR in this region. Table 2 summarizes our analyses with the Fraser-Kaufman method. We have selected locations and dates for which two AVHRR images are found on clear and hazy days without large difference in angular condition. A ruffled ocean surface has been tested with a wind velocity of 5 m s^{-1} over the sea areas, but the results have no significant difference from the case with $A_g = 0$. Locations 1-4 in Plate 1 are selected for oil-fire smoke layers. The obtained single-scattering albedo and absorption index are shown in Table 2. It is found that the tuned calibration coefficients give a larger absorption value than is obtained with the original coefficients. Since we do not know the size exponent, we assumed three values, i.e., p = 3, 4, and 5, in our simulations. Taking into account the typical ground-based value $p \approx 3.6$ found in Bushehr for oil-fire smoke events [*Nakajima et al.*, 1996a], we have $\omega \approx$ 0.73 with the original calibration coefficients, and $\omega \approx 0.70$ with the tuned calibration coefficients for both channels. The latter value is in between values from Figure 10 ($\omega \approx 0.75$) and ground-based values at Bushehr ($\omega \approx$ 0.55-0.68). Although the retrieved single-scattering albedo does not depend significantly on the assumed size exponent, the absorption index depends strongly on the size distribution, as is easily understood by the light-scattering theory of polydispersion. Table 2 indicates $\kappa \approx 0.036$ and 0.033 in channels 1 and 2 with the original calibration coefficients, and $\kappa \approx 0.044$ and 0.042 with the tuned calibration coefficients for $p \approx 3.6$.

We found thick aerosol layers in several AVHRR images that were not regarded as oil-fire smoke, such as shown by location 5 in Plate 1. Those thick aerosol layers may be sand-dust aerosol layers caused by strong wind. With this expectation, we obtain the absorption index by the Fraser-Kaufman method. To take into account the nonsphericity of the particle shape of sand-dust particles, we adopted the method of *Nakajima et al.* [1989], in which the phase function is calculated with a fictitious complex refractive index m = 1.7-0.08i, and the total extinction and scattering cross sections are calculated with m = 1.55 - κi with various values of κ. The obtained results are shown in Table 2 along with the results obtained with the ordinary Mie theory, i.e., the phase function is calculated with m = 1.55 - κi. The aerosol absorption with the nonspherical assumption is smaller than that from the Mie model. We also tested the effect of water vapor by doubling the model value and found that an error in the assumption of water vapor amount does not change our results noticeably. If we assume $p \approx 3$ found in Bushehr ($\alpha \approx$ 0.1 - 0.4) for dusty cases, we obtain $\omega \approx 0.82$ and 0.80 with the original calibration coefficients, and $\omega \approx 0.77$ and 0.74 with the tuned calibration coefficients in channels 1 and 2, respectively.

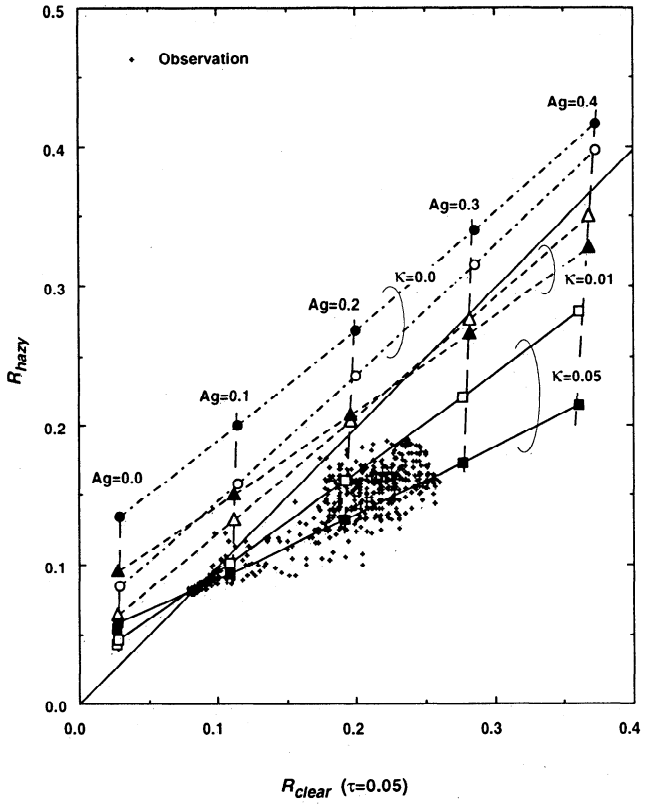

Figure 11. Fraser-Kaufman plot of reflectances of a hazy day versus those of a clear day. Three groups of theoretical lines for various ground albedos are calculated with $\kappa = 0, 0.01$, and 0.05. The optical thickness of the clear day is assumed to be 0.05, and that of the hazy day is assumed to be 0.5 and 1.0.

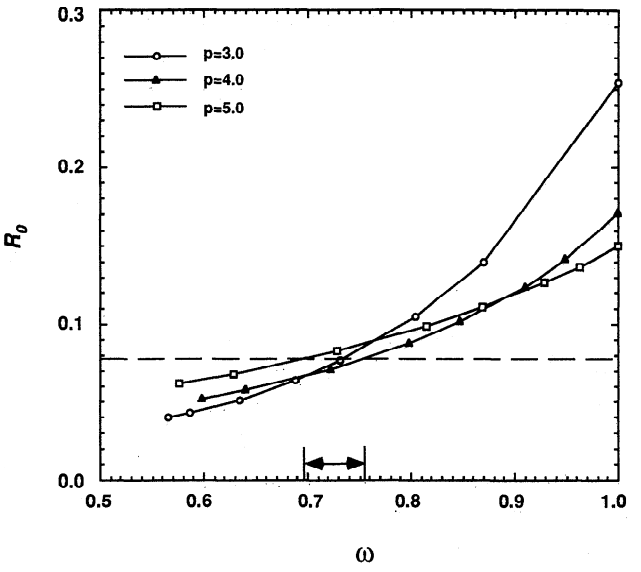

Figure 12. Dependence of the neutral reflectance on the single-scattering albedo and size distribution of aerosols.

5. Discussion and Conclusions

We have studied remote sensing of turbidity parameters $\tau_{0.5}$ and p from AVHRR data analyses. A comparison of satellite-derived values with ground-based values indicates that it is important to assume a proper aerosol absorption for adequate retrievals of turbidity parameters. A popular assumption of $\kappa = 0$ will not be suitable for successful retrievals of turbidity parameters, at least in the Persian Gulf region investigated in this study.

It has been found, however, that satellite-derived optical thickness overestimates the ground-based values, especially for large $\tau_{0.5}$, when the ground-based absorption index is assumed in our retrievals. A better agreement between satellite-derived and ground-based optical thicknesses can be found if the ground-based $\tau_{0.5}$ and/or κ have some systematic difference from suitable values for the remote sensing. This may be possible, since the location of remote sensing is not exactly same as the site of ground-based measurements. With the calibration coefficients $S_1 = 0.114$ and $S_2 = 0.122$, the aerosol optical thickness should be 20% to 100% larger than Bushehr values, as indicated by Figure 6, or the absorption index must be half of the ground-based values.

Contrary to the above explanation, it is also possible to question the other assumptions in our analyses. To have a better agreement between satellite-retrieved and ground-based optical thicknesses, we have tuned the calibration coefficients of NOAA 11 AVHRR from $S_1 = 0.114$ and $S_2 = 0.122$ to $S_1 = 0.093$ and $S_2 = 0.094$ in the summer of 1991. *Vermote and Kaufman* [1995] claimed that the center wavelength of NOAA 11 AVHRR channel 1 shifted after launch by 0.017 μm toward longer wavelengths. We have tried this assumption, but could not get substantial verification of the above conclusion. This is natural, since the shift effect is almost equivalent to $S_1 = 0.113$ and $S_2 = 0.129$ in (5), which are very similar to the original coefficients adopted in this study. *Ignatov et al.* [1995] used $S_1 = 0.110$. None of calibration coefficients in those preceding studies therefore can not bring our reflectances close to reasonable theoretical values in this study. Even though our tuned coefficients are strange when compared with those values and the preflight calibration $S_1 = 0.095$ and $S_2 = 0.090$, we have obtained more consistent results of remote sensing than with the original calibration coefficients. It should be noted in this regard that calibration constants themselves are not as well known as shown by a large range in reported values of *Ignatov et al.* [1995a].

To explain our difficulty in the calibration constant, Y. J. Kaufman (private communication,1996) has pointed out that it is highly possible that there is a systematic difference between magnitudes of phase functions with power law size distributions and with bimodal lognormal distributions at large scattering angles. There are several observations that lognormal size distributions are more realistic than power law distributions in representing the optical properties of aerosol scattering, although this is another guess without ground support data to validate our case. We should accumulate more validation studies before making a final conclusion on this problem.

Apart from a suspicion that there may be some inconsistency between our optical models and the actual situation in the Persian Gulf at that time, we state below the findings of our study with the tuned calibration coefficients.

The single-scattering albedo of oil-fire smoke was estimated as $\omega \approx 0.75$ from the simultaneous satellite data

Table 2. Parameters and Results With Fraser-Kaufman's Method of Analysis

	S_1=0.114, S_2=0.122				S_1=0.093 , S_2 = 0.094			
p	κ_1	κ_2	ω_1	ω_2	κ_1	κ_2	ω_1	ω_2
Location 1: (35.9°, 19.7°, 173.4°)$_{clear}$, (34.7°, 31.6°, 179.0°)$_{hazy}$; R_{01}=7.8, R_{02}=6.6								
3	0.0227	0.0224	0.761	0.735	0.0306	0.0297	0.761	0.706
4	0.0491	0.0457	0.727	0.727	0.0574	0.0550	0.703	0.697
5	0.0599	0.0562	0.696	0.659	0.0667	0.0644	0.674	0.629
Location 2: (36.0°, 20.8°, 174.0°)$_{clear}$, (34.8°, 32.5°, 178.4°)$_{haze}$; R_{01}=8.0, R_{02}=7.0								
3	0.0225	0.0210	0.720	0.742	0.0299	0.0286	0.694	0.710
4	0.0487	0.0438	0.728	0.734	0.0572	0.0536	0.704	0.701
5	0.0591	0.0543	0.698	0.666	0.0660	0.0630	0.676	0.634
Location 3: (36.3°, 23.1°, 174.9°)$_{clear}$, (35.2°, 34.6°, 177.4°)$_{haze}$; R_{01}=8.5, R_{02}=7.0								
3	0.0211	0.0221	0.727	0.736	0.0289	0.0294	0.697	0.707
4	0.0467	0.0444	0.734	0.732	0.0556	0.0539	0.708	0.700
5	0.0574	0.0549	0.704	0.664	0.0646	0.0635	0.680	0.632
Location 4: (36.7°, 37.2°, 176.6°)$_{clear}$, (35.7°, 37.2°, 176.6°)$_{haze}$; R_{01}=8.0, R_{02}=7.0								
3	0.0240	0.0223	0.715	0.735	0.0330	0.0296	0.683	0.706
4	0.0504	0.0452	0.723	0.729	0.0586	0.0548	0.700	0.698
5	0.0604	0.0554	0.694	0.662	0.0671	0.0638	0.672	0.631
Location 5: (Aspherical)(34.2°, 32.5°, 178.6°)$_{clear}$, (36.5°, 42.6°, 179.4°)$_{haze}$; R_{01}=11.3, R_{02}=8.0								
3	0.0085	0.0133	0.823	0.796	0.0142	0.0218	0.772	0.737
4	0.0406	0.0488	0.758	0.716	0.0534	0.0610	0.715	0.680
5	0.0515	0.0559	0.724	0.660	0.0604	0.0646	0.694	0.628
Location 5 (Mie)								
3	0.0150	0.0186	0.761	0.758	0.0192	0.0253	0.761	0.723
4	0.0335	0.0399	0.787	0.751	0.0452	0.0511	0.739	0.709
5	0.0475	0.0519	0.738	0.675	0.0569	0.0615	0.705	0.639
Location 5 (Mie, 2 × water vapor)								
3	0.0148	0.0179	0.761	0.763				
4	0.0330	0.0371	0.789	0.763				
5	0.0470	0.0494	0.740	0.685				

Angles (θ_0, θ, ϕ) for clear and hazy days, neutral reflectance R_0, absorption index κ, and single-scattering albedo ω for channels 1 and 2 of AVHRR. Values for the original and tuned calibration coefficients are shown.

analyses with ground-based turbidity parameters off the coast of Bushehr. We also estimated the single-scattering albedo with the Fraser-Kaufman method as $\omega \approx 0.70$ on the Arabian side of the Gulf. These values are larger than ground-based values at Bushehr i.e., $\omega \approx 0.55$ - 0.68. *Weiss and Hobbs* [1992] made airborne measurements of the single-scattering albedo of an intense oil-fire plume. There were two kinds of smoke, with carbon-rich small particles and with water-rich large particles, with $\omega \approx 0.4$ and 0.9, respectively. The single-scattering albedo of the well-mixed smoke plume took the value $\omega \approx 0.56$ and was not strongly dependent on the distance from fires. Satellite-derived values are larger than these values, as shown in Figure10. This fact suggests that the satellite-derived single-scattering albedo over Bushehr ($\omega \approx$ 0.75) seems to be slightly higher than expected. There might be an underestimation of the optical thickness of smoke layers with sunphotometry, as discussed in Figure 7. The indicated value in Figure 7 of $\tau_{0.5} \approx 4$ is, however, substantially larger than in situ values of $\tau_{0.5} \approx 0.7$ - 2.0 as observed by aircraft in the smoke plume [*Pilewskie and Valero,* 1992], suggesting it might be difficult to explain by this reasoning. Another explanation may be a strong vertical inhomogeneity of aerosol optical characteristics in the smoke layer. If there were fewer light-absorption aerosols near the top layer, for example, the radiation will be much more effectively scattered to space than in the homogeneous aerosol layer case that we have assumed. *Ferrare et al.* [1990] found that the single-scattering albedo of forest fire aerosols can increase, as high as 0.9, owing to water vapor absorption during transport. It should be noted that the transport time will be longer than 1 day in the smoke event at Bushehr in weak wind conditions [*Nakajima et al.*, 1996a].

We have analyzed one more case at location 5 of Plate 1 with the Fraser-Kaufman method and got κ = 0.0192 and 0.0253 ($\omega \approx 0.77$ and 0.74) in channels 1 and 2 of AVHRR, respectively. If this is a sand-dust layer, a tendency for larger absorption at shorter wavelengths is reasonable, as indicated by spectral refractive indices of Saharan and Asian dusts.

Our values are, however, smaller than those of Saharan dust (κ= 0.013, 0.0033, 0.0020 at λ = 0.35, 0.5, 0.7 μm) [*Carlson and Benjamin,* 1980] and Chinese yellow sand dust (κ = 0.0080, 0.0052, 0.0037 at λ = 0.35, 0.5, 0.7 μm) [*Ohta,* 1987]. The layer observed at location 5 may not be a sand-dust layer, but an anthropogenic aerosol layer with soot particles or a mixture with sand-dust particles. It is difficult to draw a conclusion on the origin of aerosols without accompanying chemical data.

It should be noted in Table 2 that the inclusion of the nonspherical particle effect is important for estimating the relevant parameters of sand particles with adequate accuracy. Recent nonspherical scattering theories [e.g., *Mischenko et al.*, 1995] will be promising for better assumption of aerosol optical characteristics for the use of remote sensing.

Through all the analyses in the present study, light absorption played an important role in aerosol retrievals in this region. At the same time, we experienced that accurate retrievals of aerosol absorption is difficult. It should be noted that reported aerosol absorption indices of Tsuson, Arizona, as one of the most well-investigated cases, range as large as κ= 0.0 - 0.030, partly owing to differences in measurement methods [*King*, 1979; *Spinhirne et al.*, 1980; *Reagan et al.*, 1980; *Ohta et al.*, 1996]. It is therefore vital to find a reliable method of retrieving aerosol absorption. In this regard, simultaneous airborne measurements of aerosols and radiation will be helpful for satellite data analyses to eliminate ambiguity such as that experienced in this study [e.g., *Wendisch et al.*, 1996]. A new network of sky radiometer under development [*Holben et al.*, 1996; *Nakajima et al.*, 1996b] is also noteworthy for providing better aerosol optical characteristic information from the ground. Remote sensing techniques should be closely compared with in situ sampling techniques for deriving single-scattering albedo [e.g., *Hänel*, 1988, 1994].

Those aerosol retrievals should be linked in the future with cloud microphysical retrievals to estimate the cloud-aerosol interaction strength as well as aerosol direct forcing. New-generation satellite radiometers, such as Earth Obseving Satellite moderate-resolution imaging spectrometer (EOS MODIS) [*King et al.*, 1992] and ADEOS II Global Imager (GLI), should be used to realize better retrievals of aerosols and clouds with their 36 channels of good sensitivity and dynamic range.

Acknowledgments. We are grateful to Tadahiro Hayakasa of Tohoku University and the staffs of Department of the Environment of Iran for getting the ground-based radiation data. One of the authors is also grateful to S.-T. Tsay of NASA Goddard Space Flight Center and Peter Pilewskie of NASA Ames Research Center for providing the information on airborne measurements conducted in the Persian Gulf region in May 1991.

References

Cahalan, R. F., The Kuwait oil fires as seen by Landsat, *J. Geophys. Res.*, *97*, 14,565-14,571, 1992.

Carlson, T. N., and S. G. Benjamin, Radiative heating rates for Saharan dust, *J. Atmos. Sci.*, *37*, 193-213, 1980.

Charlson, R. J., S. E. Schwartz, J. M. Hales, R. D. Cess, J. A. Coakley Jr., J. E. Hansen, and D. J. Hofmann, Climate forcing by anthropogenic aerosols, *Science*, 255, 423-430, 1992.

Coakley, J. A., Jr., R, L. Bernstein, and P. A. Durkee, Effect of ship-track effluents on cloud reflectivity, *Science*, *237*, 1020-1022, 1987.

Duce, R. A., Sources, distributions, and fluxes of mineral aerosols and their relationship to climate, in *Aerosol Forcing of Climate*, edited by R. J. Charlson and J. Heintzenberg, 43-72, John Wiley, New York 1995.

Ferrare, R. A., R. S. Fraser, and Y. J. Kaufman, Satellite measurements of large-scale air pollution: Measurements of forest fire smoke, *J. Geophys. Res.*, *95*, 9911-9925, 1990.

Fraser, R. S., and Y. J. Kaufman, The relative importance of aerosol scattering and absorption in remote sensing, *IEEE Trans. Geosci. Remote Sens.*, *23*, 625-633, 1985.

Gordon, H. R., and A. Y. Morel, Remote assessment of ocean color for interpretation of satellite visible imagery, in *Lecture Notes on Coastal and Estuarine Studies*, vol. 4, 114 pp. Springer-Verlag, New York, 1983.

Gordon, H. R., and M. Wang, Retrieval of water-leaving radiance and aerosol optical thickness over the oceans with SeaWiFS: A preliminary algorithm, *Appl. Opt.*, *33*, 443-452, 1994.

Han, Q., W. B. Rossow, and A.A. Lacis, Near-global survey of effective droplet radii in liquid water clouds using ISCCP data, *J. Clim.*, *7*, 465-497, 1994.

Hänel, G., Single scattering albedo, asymmetry parameter, apparent refractive index, and apparent soot content of dry atmospheric particles, *Appl. Opt.*, *27*, 2287-2295, 1988.

Hänel, G., Optical properties of atmospheric particles: Complete parameter sets obtained through polar photometry and an improved inversion technique, *Appl. Opt.*, *33*, 7187-7199, 1994.

Hayasaka, T., T. Nakajima, S. Ohta, and M. Tanaka, Optical and chemical properties of urban aerosols, *J. Atmos. Environ.*, *26A*, 2055-2062, 1992.

Holben, B. N., T. E. Eck, I. Slutsker, D. Tanré, J. P. Buiss, A. Setzer, E. Vermote, J. A. Reagan, and Y. J. Kaufman, Automatic sun and sky scanning radiometer system for network aerosol monitoring, *Remote Sens. Environ.*, in press, 1996.

Husain, T., Kuwait oil fires - Modelling revisited, *Atmos. Environ.*, *28*, 2211-2226, 1994.

Ignatov, A. M., L. L. Stowe, S. M. Sakerin, and G. K. Korotaev, Validation of the NOAA/NESDIS satellite aerosol product over the North Atlantic in 1989, *J. Geophys. Res.*, *100*, 5123-5132, 1995a.

Ignatov, A., L. Stowe, R. Singh, S. Sakerin, D. Kabanov, and I. Dergileva, Validation of NOAA/AVHRR aerosol retrievals using sun-photometer measurements from R/V Akademik Vernadsky in 1991, *Adv. Space Res.*, *16*, 95-98, 1995b.

Kaufman, Y. J., and B. N. Holben, Calibration of the AVHRR visible and near-IR bands by atmospheric scattering, ocean glint and desert reflection, *Int. J. Remote Sens.*, *14*, 21-52, 1993.

Kaufman, Y. J., and T. Nakajima, Effect of Amazon smoke on cloud microphysics and albedo - Analysis from satellite imagery, *J. Appl. Meteorol.*, *32*, 729-744, 1993.

Kidwell, K. B., NOAA polar orbiter data (TIROS-N, NOAA-6, NOAA-7, NOAA-8, NOAA-9, NOAA-10, and NOAA-11) users guide, NOAA Natt. Environ. Satellite Data and Inf. Serv., Washington, D.C., 1988.

Kiehl, J. T., and B. P. Briegleb, The relative roles of sulfate aerosols and greenhouse gases in climate forcing, *Science*, *260*, 311-314, 1993.

Kiehl, J. T., and H. Rodhe, Modeling geographical and seasonal forcing due to aerosols, in *Aerosol Forcing of Climate*, edited by R. J. Charlson and J. Heintzenberg, pp. 281-286, John Wiley, New York, 1995.

King, M. D., Determination of the ground albedo and the index of absorption of atmospheric particulates by remote sensing, II, Application, *J. Atmos. Sci.*, *36*, 1072-1083, 1979.

King, M. D., Y. J. Kaufman, W. P. Menzel, and D. Tanre, Remote sensing of cloud, aerosol, and water vapor properties from the Moderate Resolution Imaging Spectrometer (MODIS), *IEEE Trans. Geosci. Remote Sens.*, *30*, 2-27, 1992.

Kneizys, F. X., E. P. Shettle, L. W. Abreu, J. H. Chetwynd, G. P. Anderson, W. O. Gallery, J. E. A. Selby, and S. A. Clough, Users guide to LOWTRAN 7, Rep. *AFGL-TR-88-0177*, Air Force Geophys. Lab., Hanscom AFB, Mass., 1986.

Langner, J., H. Rodhe, P. J. Crutzen, and P. Zimmermann, Anthropogenic influence on the distribution of tropospheric sulphate aerosol, *Nature*, *359*, 712-716, 1992.

Limaye, S. S., S. A. Ackerman, P. M. Fry, M. Isa, H. Ali, G. Ali, A. Wright, and A. Rangno, Satellite monitoring of smoke from the

Kuwait oil fires, *J. Geophys. Res.*, *97*, 14,551-14,563, 1992.
McQueen, J. T., and R. R. Draxler, Evaluation of model back trajectories of the Kuwait oil fires smoke plume using digital satellite data, *Atmos. Environ.*, *28*, 2159-2174, 1994.
Mischenko, M., D.W.Mackowski, and L.D.Travis, Scattering of light by bispheres with touching and separated components, *Appl. Opt.*, *34*, 4589-4599, 1995.
Mitchell, J. F. B., T. C. Johns, J. M. Gregory, and S. F. B. Tett, Climate response to increasing levels of greenhouse gases and sulphate aerosols, *Nature*, *376*, 501-504, 1995.
Nakajima, T. Y., and T. Nakajima, Wide-area determination of cloud microphysical properties from NOAA AVHRR measurements for FIRE and ASTEX regions, *J. Atmos. Sci.*, *52*, 4043-4059, 1995.
Nakajima, T., and M. Tanaka, Effect of wind-generated waves on the transfer of solar radiation in the atmosphere-ocean system, *J. Quant. Spectrosc. Radiat. Transfer*, *29*, 521-537, 1983.
Nakajima, T., and M. Tanaka, Matrix formulations for the transfer of solar radiation in a plane-parallel scattering atmosphere, *J. Quant. Spectrosc. Radiat. Transfer*, *35*, 13-21, 1986.
Nakajima, T., and M. Tanaka, Algorithms for radiative intensity calculations in moderately thick atmospheres using a truncation approximation, *J. Quant. Spectrosc. Radiat. Transfer*, *40*, 51-69, 1988.
Nakajima, T., M. D. King, J. D. Spinhirne, and L. F. Radke, Determination of the optical thickness and effective radius of clouds from reflected solar radiation measurements. II, Marine stratocumulus observations, *J. Atmos. Sci.*, *48*, 728-750, 1991.
Nakajima, T., M. Tanaka, M. Yamano, M. Shiobara, K. Arao, and Y. Nakanishi, Aerosol optical characteristics in the yellow sand events observed in May, 1982 in Nagasaki, II, Model, *J. Meteorol. Soc. Jpn.*, *67*, 279-291, 1989.
Nakajima, T., T. Hayasaka, A. Higurashi, G. Hashida, N. Moharram-Nejad, Y. Najafi, and H. Valavi, Aerosol optical properties in the Iranian region obtained by ground-based solar radiation measurements in the summer of 1991, *J. Appl. Meteorol.*, 35, 1265-1278,1996a.
Nakajima, T., G. Tonna, R. Rao, Y. Kaufman, and B. Holben, Use of sky brightness measurements from ground for remote sensing of particulate polydispersions, *Appl. Opt.*, in press, 1996b.
Ohta, S., Black carbon and soil particles and their environmental effects, *Rep. of Environ. Sci. Res. B316-R11-6*, pp.78-107, Min. of Art and Educ., 1987.
Ohta, S., M. Hori, N. Murao, S. Yamangaata, and K. Gast, Chemical and optical properties of lower tropospheric aerosols measured at Mt. Lemmon in Arizona. *J. Environ. Eng.*, *2*, 67-78, 1996.
Penner, J. E., Carbonaceous aerosols influencing atmospheric radiation, *Aerosol Forcing of Climate*, edited by R. J. Charlson and J. Heintzenberg, pp. 91-108, John Wiley, New York, 1995.
Pilewskie, P., and F. P. J. Valero, Radiative effects of the smoke clouds from the Kuwait oil fires, *J. Geophys. Res.*, *97*, 14,541-14,544, 1992.
Plass, G. N., G. W. Kattawar, and F. E. Catchings, Matrix operator theory of radiative transfer, 1, Rayleigh scattering, *Appl. Opt.*, *12*, 314-329, 1973.
Qiu, J., Z. Xiuji, S. Jinhui, X. Qilin, and Z. Jinding, Simultaneous determination of the aerosol size distribution, refractive index, and surface albedo from radiance data in *Atmospheric Radiation: Progress and Process*, edited by K.-N. Liou and Z. Xiuji, pp. 550-556, Science Press, 1987.
Radke, L. F., J. A. Coakley Jr., and M. D. King, Direct and remote sensing observations of the effects of ships on clouds, *Science*, *246*, 1146-1149, 1989.
Rao, C. R. N., L. L. Stowe, E. P. McClain, and J. Sapper, Development and application of aerosol remote sensing with AVHRR data from the NOAA satellites, in *Aerosols and Climate.*, edited by P. V. Hobbs and M. P. McCormick, pp. 69-79. A. Deepak, Hampton, Va., 1988.
Reagan, J. A., D. M. Byrne, M. D. King, J. D. Spinhirne, and B. M. Herman, Determination of the complex refractive index and size distribution of atmospheric particulates from bistatic-monostatic lidar and solar radiometer measurements, *J. Geophys. Res.*, *85*, 1591-1599, 1980.
Ruggaber, A., R. Dlugi, and T. Nakajima, Modelling radiation quantities and photolysis frequencies in the troposphere, *J. Atmos. Chem.*, *18*, 171-210, 1994.
Spinhirne, J. D., J. A. Reagan, and B. M. Herman, Vertical distribution of aerosol extinction cross section and inference of aerosol imaginary index in the troposphere by lidar technique, *J. Appl. Meteorol.*, *19*, 426-438, 1980.
Stowe, L. L., R. M. Carey, and P. P. Pellegrino, Monitoring the Mt. Pinatubo aerosol layer with NOAA/11 AVHRR data, *Geophys. Res. Lett.*, *19*, 159-162, 1992.
Tanaka, M., T. Takamura, and T. Nakajima, Refractive index and size distribution of aerosols as estimated from light scattering measurements, *J. Clim. Appl. Meteorol.*, *22*, 1253-1261, 1983.
Tanaka, M., T. Hayasaka, and T. Nakajima, Airborne measurement of optical properties of tropospheric aerosols over an urban area, *J. Meteorol. Soc. Jpn.*, *68*, 335-345, 1990.
Taylor, K. E., and J. E. Penner, Response of the climate system to atmospheric aerosols and greenhouse gases, *Nature*, *369*, 734-737, 1994.
Vermote, E., and Y.J. Kaufman, Absolute calibration of AVHRR visible and near infrared channels using ocean and cloud views, *Int. J. Remote Sens.*, *16*, 2317-2340, 1995.
Weiss, R. E., and P. V. Hobbs, Optical extinction properties of smoke from the Kuwait fires. *J. Geophys. Res.*, *97*, 14,537-14,540, 1992.
Wendisch, M., S. Mertes, A. Ruggaber, and T. Nakajima, Vertical profiles of aerosol and radiation under cloudless conditions: Measurements and radiative transfer calculations. *J. Appl. Meteorol.*, in press, 1996.

A. Higurashi and T. Nakajima, Center for Climate System Research, University of Toikyo, 4-6-1 Komaba, Meguro-ku, Tokyo 153, Japan. (e-mail:teruyuki@ccsr.u-tokyo.ac.jp)

(Received February 12, 1996; revised June 3, 1996; accepted June 3, 1996.)